15TH IEA HEAT PUMP CONFERENCE
MAY 26–29, 2026 | HOFBURG
VIENNA 2026
DECARBONISATION THROUGH INNOVATION

Investigation of a constructive geostatistical method to assimilate unused conventional data during geothermal drilling for hydraulic conductivity profiling

Olivier Brisebois[a], Dany Lauzon[a], Philippe Pasquier[a]

[a]Polytechnique Montreal, 2500 Polytechnique Road, Montreal, H3T 0A3, Canada

Abstract

Open geothermal systems, such as standing column wells, can benefit from a thorough characterization of the geological and hydrogeological properties of the fractured rock formation in which it is installed. Methods providing depth-dependent properties typically require additional, and often expensive, field investigations. Therefore, characterizing the vertical distribution of hydrogeological properties in a geothermal borehole requires alternative approaches that provide rapid and cost-effective insights. This study proposes to analyze the information collected routinely during exploratory drilling. One potential data source is flow rates measured at the borehole outlet during air-injection drilling. These measurements, which are relatively inexpensive to acquire during the investigation phase, may provide valuable information on fracture networks that can be used to infer the hydraulic conductivity profile with depth. To this end, a constructive geostatistical data-assimilation technique is used to estimate the hydraulic conductivity of fractured rock as a function of depth, using fluid flow rate measurements obtained during drilling. The method assimilates flow rate data by optimizing the distribution of fracture hydraulic conductivity. A likelihood-based objective function accounts for uncertainties in in-situ observations, enabling a probabilistic interpretation of fracture characteristics. Using the observed flow rate as input, the geostatistical algorithm estimates the depth-dependent hydraulic conductivity profile and identifies major fractures intersected during drilling. These profiles are then used to simulate transfer functions, offering insight into how fracture networks affect geothermal heat transfer. Two demonstrations are presented: a synthetic numerical model constructed from realistic geological constraints, and a real-world application in which flow rates were measured during the investigation phase of a geothermal system project in Mirabel, Quebec, Canada. Results from both cases indicate that flow rates measured at the borehole outlet during air-injection drilling provide some information on the depth-dependent hydraulic conductivity profile and help identify zones of low- and high-permeability fractures.

Keywords: Ground heat exchanger; Standing column well; Bayesian geostatistical inversion; Transfer function; Flow rate assimilation; Coupled hydro-thermal simulation

1. Introduction

Uncertainty arising from the heterogeneous nature of geological materials remains a fundamental challenge in subsurface characterization and modeling, especially for fluid flow [1]. Spatial variability in hydraulic conductivity controls the movement of fluids and heat in the subsurface, which are key factors in geothermal energy extraction. Therefore, accurate characterization of hydraulic conductivity is critical to improving predictive models of flow and transport processes, particularly in fractured rock, where flow occurs through complex, spatially discontinuous fracture networks [2].

Numerous in-situ and laboratory techniques have been developed to estimate average hydraulic conductivity, including slug tests, pumping tests [3], hydraulic tomography [4], and core-based permeability measurements [5]. Although well established, these methods are often costly, time-consuming, and limited in spatial resolution. In fractured media, the estimation of representative hydraulic conductivity values is further complicated by the anisotropy and spatial variability of fracture aperture, connectivity, and orientation [6-7]. To overcome these limitations, indirect geophysical methods such as acoustic and optical televiewing [8], nuclear magnetic resonance [9], electrical resistivity logging [10], flow velocimetry [11], and injection logging

[12] have been used to obtain depth-dependent information. These techniques can delineate fractured zones and provide localized estimates of hydraulic conductivity or porosity. However, they generally require specialized equipment, additional field operations, and post-processing expertise. The resulting costs and logistical constraints limit their application during routine geothermal site characterization.

Accurate estimation of hydraulic conductivity distributions is critical in open geothermal systems, where the efficiency of heat transfer depends on the interaction between the circulating fluid and the surrounding rock formation. Among ground heat exchangers, standing column wells (SCW) constitute a promising configuration that combines the advantages of open- and closed-loop systems [13]. A SCW typically consists of a deep, uncased borehole drilled into competent bedrock, from which groundwater is pumped, circulated through a heat pump, and then reinjected at the base of the borehole via an injection pipe. During peak heating or cooling conditions, part of the pumped water can be discharged to an auxiliary injection well, a process known as bleed, which induces a drawdown and enhances advective heat transfer in the surrounding fracture network [14-15]. These features make SCWs particularly suitable for urban or space-constrained environments, where they offer significant reductions in cost and installation footprint compared to conventional closed-loop systems [13].

Predicting the performance of a geothermal well, such as a SCW, requires modeling the transient temperature evolution of the circulating fluid in response to a variable heat load. This dynamic response can be represented by a thermal transfer function, which expresses the temporal relationship between an imposed unit heat load and the resulting temperature change at a specified location, typically at the well outlet [13, 16-17]. Therefore, transfer functions encapsulate the coupled thermo-hydraulic behavior of the subsurface and can be convolved with load histories to estimate system performance without rerunning full numerical simulations. They are indispensable for the design, optimization, and interpretation of thermal response tests performed on SCWs.

However, constructing accurate transfer functions for SCWs remains a challenge owing to the uncertainties involved in characterizing the hydraulic conductivity profile and fracture network within the host formation. In homogeneous porous media, analytical formulations such as the infinite line-source model provide reliable long-term solutions [18]. Yet, in fractured bedrock, advection through discrete fractures dominates over conduction, and the thermal response becomes highly dependent on fracture geometry and hydraulic conductivity contrasts [19-20]. Pasquier et al. [13] highlighted that even a single productive fracture intersecting a SCW can substantially alter temperature recovery rates, demonstrating the sensitivity of geothermal performance to subsurface heterogeneity. To capture these effects, recent numerical studies have coupled groundwater flow and heat transfer equations using finite-element or finite-volume methods [13, 17]. While such simulations yield accurate transfer functions, they are computationally intensive and require detailed site-specific hydraulic data that are often unavailable or costly to obtain.

These constraints underscore the need for efficient inversion strategies capable of inferring hydraulic properties from indirect or routinely measured data. Drilling operations in fractured bedrock naturally produce valuable information in the form of flow rate variations at the borehole outlet. During air-injection drilling, these discharge rates reflect the relative hydraulic conductivity of fractures intersected by the borehole. Because they are typically recorded to estimate the water flow rates obtainable in the well and determine the most conductive zones, such measurements can be repurposed to infer depth-dependent hydraulic conductivity. Despite their potential, these data are rarely exploited beyond basic lithological logging. Integrating them into a formal inversion framework could yield new insights into the hydraulic profile without necessitating additional field campaigns.

In this context, the present study investigates the use of flow rate measurements acquired during drilling to infer the vertical distribution of hydraulic conductivity in fractured rock. The approach is based on a geostatistical inversion method [21] that assimilates observed flow rates to optimize the spatial distribution of fracture hydraulic conductivity and, indirectly, the equivalent hydraulic conductivity of the system. The method is evaluated using two case studies: a synthetic case, in which the reference fracture hydraulic conductivities are known, and a real case, in which only flow rate data collected during drilling are available and fracture hydraulic properties must be inferred.

2. Methodology

2.1. Site Description

The data used in this study were collected during the design of a geothermal system comprising five SCWs and one reinjection well installed at an elementary school in Mirabel, eastern Canada. The objective of the project was to demonstrate the performance and reliability of SCWs for institutional buildings operating in cold climates. The site has undergone a thorough characterization of its hydrogeological and thermal properties [20].

Among the wells drilled on the site, borehole PE-20-01 was selected as the primary investigation site for this study, where a dedicated pumping test was conducted to characterize the local hydrogeological conditions [20]. The configuration and location of PE-20-01 on the school property are shown in Figure 1. The borehole intersects three distinct lithological units identified from rock cuttings collected during drilling, representing a typical stratigraphic sequence of the St. Lawrence Lowlands [22]. The uppermost 10.05 m consists of glacial till deposits. Beneath the till, the borehole penetrates the Theresa Formation of the Beekmantown Group, composed primarily of sandy dolomite. At a depth of 99.06 m, lithology transitions into the Cairnside Formation of the Potsdam Group, a quartz arenite that extends to the bottom of the borehole at 133.20 m [22]. A steel casing was installed from the surface to the depth of competent bedrock to hydraulically isolate the shallow surface water from the deeper groundwater system.

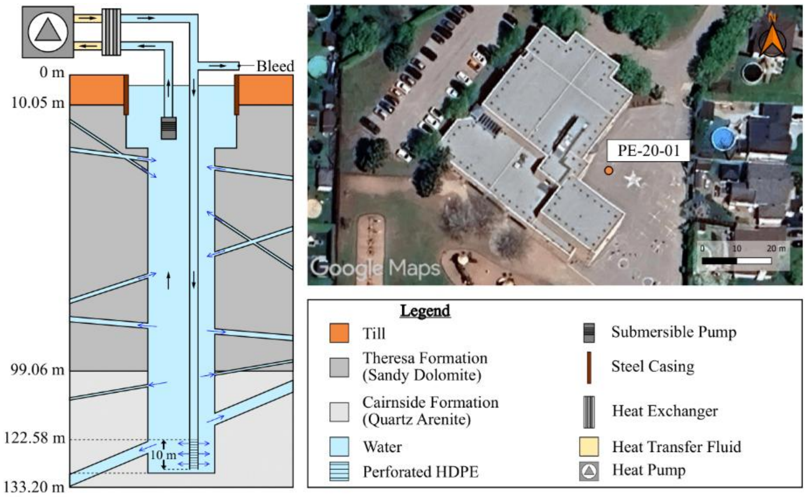

Figure 1. Schematic representation and location of SCW PE-20-01.

2.2. Numerical Modeling and Case Study Design

Two finite-element axisymmetric models were implemented in *COMSOL Multiphysics* [23] to simulate the hydrogeological behavior and thermal response of the system. The first model simulates the flow rate measured during drilling under the imposed boundary and hydraulic conditions. It is used to infer the fracture's hydraulic conductivity from observed flow rates. The second model simulates heat transfer using the resulting fracture's hydraulic conductivity to generate the corresponding thermal transfer functions, thereby linking the inferred hydraulic properties to the SCW's performance. It then assesses how improved characterization of fracture hydraulic properties influences the thermal response.

2.2.1. Hydrogeological Model

The hydrogeological finite-element model was designed to simulate the flow rate measured at the borehole outlet during drilling. The flow rate depends on the drilling depth, making the process inherently iterative. Therefore, to simulate a series of *n* flow rates, an equal number of models were run, each corresponding to the geological conditions at a specific drilling depth. Figure 2 illustrates this process for the ninth iteration, in which the simulated domain includes only the first nine 7.62 m intervals, corresponding to a borehole depth of 68.58 m.

The spacing between model runs was defined based on the 25 ft (7.62 m) length of the drilling rods used in borehole PE-20-01. At each run, the model represents an additional 7.62 m drilling increment, within which a hypothetical horizontal fracture is assumed at the midpoint of the newly drilled section. This equivalent fracture is considered to represent the combined effects of multiple fractures with varying orientations, apertures, and hydraulic conductivities. This simplification allows for a direct relationship between changes in flow rate and the inferred hydraulic conductivity, while acknowledging the inherent limitation in the spatial resolution of the current drilling-based measurement method. As previously stated, the model was run at each drilling step, generating a cumulative flow rate function. The objective is therefore to infer, through inversion, the hydraulic conductivity associated with each equivalent fracture from the measured increase in flow rate at each depth.

In practice, the simulated flow rates are compared with discharge measurements obtained directly in the field. Two approaches are commonly used during drilling. The first and least precise relies on visual estimation, which can be heavily influenced by the driller's experience and judgment. The second involves manual measurement of discharge between drilling rods using a bucket and a stopwatch, offering improved precision but remaining subject to several limitations, such as incomplete water capture and the effects of air injection or drilling fluids on the observed discharge. For borehole PE-20-01, the second method was used to measure the flow rate. However, these measurements remain prone to uncertainty and must be explicitly accounted for during the inversion process to avoid overfitting the inferred hydraulic conductivities. We use a geostatistical approach to handle these uncertainties, as described later.

With a total drilled depth of 133.20 m, 18 discharge measurements were obtained. The first data point was excluded from the analysis because it corresponds to a depth in the soil where no open fractures can exist. The boundary conditions shown in Figure 2 were validated using the Thiem equation for a homogeneous, fracture-free model to ensure consistency with classical analytical solutions [24].

2.2.2. Thermal Model

The modeling strategy employed to simulate the coupled thermal response of PE-20-01 is based on Beaudry et al. [19], and a thermal model of PE-20-01 was built by Robert et al. to evaluate the impact of layered heterogeneity on the interpretation of thermal response tests performed on a SCW [20]. Some modifications to the thermal model built by Robert et al. were made to align with our hydrogeological model. Two distinct sets of boundary conditions were applied, as illustrated in Figure 2. The hydrogeological boundary conditions enforce vertical flow within both the injection pipe and the borehole, while also inducing horizontal flow in the fractured aquifer. The thermal boundary conditions impose a unit thermal impulse of 1 °C at the SCW inlet. This is achieved by first evaluating the entering water temperature in the heat exchanger (EWT), and then prescribing the leaving water temperature of the heat exchanger as $LWT_{in} = EWT_{out} + 1\ °C$. Additional boundary conditions establish a uniform initial temperature of 0 °C and an initial hydraulic head of 0 m. This configuration enables the generation of a thermal transfer function, which can subsequently be convolved with a building's thermal load to evaluate the system's response [16]. As the transfer function is controlled solely by the borehole's hydrogeological and thermal properties, the analysis relies on the ensemble of functions to represent fracture-related variability. The geostatistical framework supplies multiple realizations of the hydraulic parameters, each producing its own transfer function, and this ensemble is used to quantify how hydraulic variability influences the predicted system performance.

As shown in Figure 2, the thermal model extends to a depth of 127.58 m. The domain is truncated near the midpoint of the perforated section of the injection pipe, and the flow entering the EWT inlet is constrained to equal the flow exiting the LWT outlet. This configuration prevents numerical instabilities that may arise near the bottom of the borehole. Because the deepest fracture lies below the truncated section, this choice removes its influence from the thermal model; however, in practice, such a fracture would contribute to SCW thermal performance. Since all transfer functions were generated using the same simplification, the effect on comparative analyses is considered negligible.

2.2.3. Design of the Case Studies

A traditional way to evaluate the performance of a new geostatistical approach is to construct a synthetic case in which all parameters can be controlled. This approach helps validate the methodology and facilitates its application to real-world cases. Accordingly, two versions of the case study were developed. Both models share the same geological framework, but their hydrogeological properties —specifically, the fracture hydraulic conductivity, the mean hydraulic conductivity of the surrounding matrix and the borehole effective porosity—were adjusted to represent two distinct scenarios.

The first scenario corresponds to a synthetic case in which the fracture conductivities, water discharge during drilling, and boundary conditions are fully known. The second scenario represents the real case, where only the water discharge data recorded during drilling are available. In this case, *a priori* information is required to constrain the numerical model associated with the real data.

Both the synthetic and real studies share the hydrogeological and thermal properties assigned to the materials composing the borehole structure, which are summarized in Table 1. These parameter values are based on field observations and informed estimates drawn from previous investigations at the site [20], as well as from studies of the lithological and hydraulic characteristics of the St. Lawrence Lowlands [25].

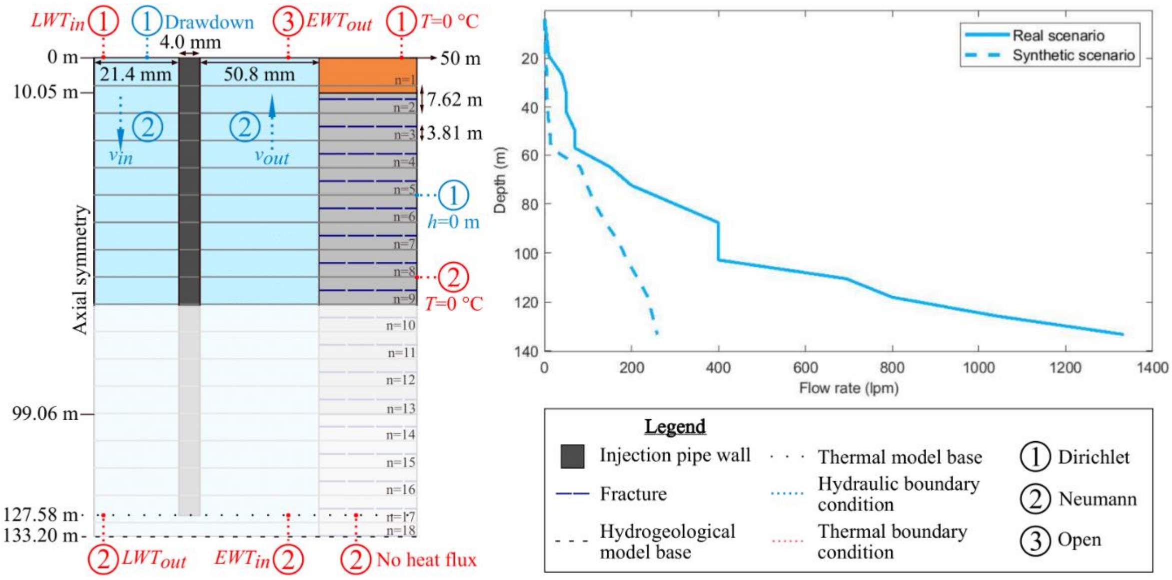

Figure 2. Numerical finite-element models of borehole PE-20-01 and their boundary conditions at the 9th iteration. The top-right panel shows the reference flow rates for both the synthetic and real scenarios. Additional legend details are provided in Figure 1. No-flow boundaries are imposed at the top and bottom of the models.

Table 1. Hydrogeological and thermal parameters incorporated in the finite-element models of PE-20-01. [a]From [20]; [b]From [25]; [c]Educated guess.

Properties	Units	Soil	Theresa Formation	Cairnside Formation	HDPE
Thickness	m	10.05[a]	89.01[a]	34.14[a]	-
Density	kg m^{-3}	2700[a]	2700[a]	2700[a]	950[a]
Matrix porosity	%	20[a]	1[c]	1[c]	0.001[a]
Matrix hydraulic conductivity	m/s	1E-8[c]	1E-8[c]	1E-7[c]	1E-12[c]
Specific heat capacity	J kg^{-1} K^{-1}	850[a]	857[b]	809[b]	2400[a]
Thermal conductivity	W m^{-1} K^{-1}	2.7[a]	3.6[b]	5.9[b]	0.42[a]

The main difference between the two studies lies in the set of *a priori* values used for the drawdown and the fracture hydraulic properties. For the synthetic scenario, flow rates were simulated using a random vector of fracture hydraulic conductivities and a drawdown distribution generated from a single geostatistical realization using the spectral turning band methods (STBM) algorithm [26]. In contrast, the real scenario uses drawdown values obtained from flow rate measurements recorded during drilling operations, from which *a priori* information on drawdown is constructed. Figure 2 illustrates the boundary conditions applied in both the hydrogeological and thermal finite-element models, along with the reference flow profiles for the synthetic and real scenarios.

For both the synthetic and real scenarios, the expected fracture hydraulic conductivity and drawdown at each interval were defined as *a priori* information for the inversion algorithm. The *a priori* values of fracture hydraulic conductivity were derived from typical ranges reported for the lithologies encountered by Nastev et al. [27] and their expected evolution with increasing flow rate, as shown in Table 2. For each lithological unit, mean fracture conductivities were selected such that the resulting average layer conductivity was representative of the corresponding formation. In addition, because a pumping test was performed in borehole PE-20-01, the mean hydraulic conductivity of the borehole was assumed to be known.

Accordingly, a reference value of 9.0×10^{-5} m/s was chosen for the synthetic scenario, while the measured value of 6.5×10^{-5} m/s was adopted for the real scenario. The mean fracture hydraulic conductivities were subsequently adjusted to align with the pumping test results. Furthermore, using the effective porosity ranges reported by Tran Ngoc et al. [28], total fracture apertures were assigned for each 7.62 m interval. The real scenario uses mean effective porosity values for each lithology based on these published ranges. In contrast, the synthetic scenario represents a slightly more fractured aquifer to test the inversion algorithm's sensitivity. The reference values of Table 2 are not intended to be precisely reproduced by the algorithm but rather to serve as guiding estimates for the expected order of magnitude of the fracture hydraulic conductivities.

Table 2. Hydrogeological parameters of the fractures used in synthetic and real scenarios. [a]From [20]; [b]From [27]; [c]From [28]; [d]Educated guess.

Scenario	Properties	Units	Soil	Theresa Formation	Cairnside Formation
Synthetic	Mean fracture hydraulic conductivity	m/s	1E-8[d]	[2.54E-4, 4.57E-3] [d]	[2.49E-3, 1.39E-2] [d]
	Total fracture aperture (per 7.62 m)	mm	0	150	275
	Effective porosity	%	20[a]	3.02 [c]	5.03 [c]
	Mean layer hydraulic conductivity	m/s	1E-8	2.96E-5[b]	2.54E-4[b]
Real	Mean fracture hydraulic conductivity	m/s	1E-8[d]	[8.57E-5, 6.93E-3] [d]	[3.81E-3, 1.43E-2] [d]
	Total fracture aperture (per 7.62 m)	mm	0	88	160
	Effective porosity	%	20[a]	2.19 [c]	3.34 [c]
	Mean layer hydraulic conductivity	m/s	1E-8	2.83E-5[b]	1.66E-4[b]

Because the drawdown cannot be measured during drilling, it was treated as an optimized variable within a prescribed range. For the synthetic scenario, a normal distribution of potential drawdown values was transformed into a cumulative distribution function (CDF), allowing drawdown to increase progressively between 0 m and 0.5 m at each interval. In the real scenario, however, the drawdown was observed to follow a trend similar to that of the flow rate evolution. Therefore, the CDF was modified to reproduce this behavior. A simplified drawdown evolution, as used in the synthetic case, proved inadequate for the real scenario, as preliminary sensitivity analyses showed that drawdown strongly affects the simulated flow rates. Because drawdown varies at each drilling step in practice, assuming a linear drawdown evolution would be unrealistic.

2.3. Bayesian Geostatistical Framework

Geostatistical simulation generates multiple equally probable realizations of subsurface properties, allowing the spatial uncertainty and heterogeneity of geological media to be quantified and propagated through models. When combined with data assimilation techniques, these simulations are iteratively constrained by observed data, reducing uncertainty and producing models that are both geologically realistic and consistent with field measurements. In this study, a Bayesian geostatistical simulation framework is used to generate an ensemble of hydraulic conductivity fracture profiles that reproduce the observed water flow rates.

We employ the Sequential Spectral Turning Bands Method (S-STBM) proposed by Lauzon and Marcotte [21]. This geostatistical inversion algorithm calibrates Gaussian random fields by sequentially adding spectral components that minimize a defined objective function (OF). To accelerate computation, the formalism introduced by Lauzon [29] is adopted, which optimizes groups of spectral components simultaneously rather than individually. The result is a Gaussian random field that honors the measured data while preserving the statistical and spatial characteristics of the underlying geological structure. The hydraulic conductivity is modeled in logarithmic form (log K), allowing the parameter field to be represented as a Gaussian random variable for inversion. In contrast, drawdown values are treated as uniformly distributed and transformed into a normal distribution using their CDFs mapped to the standard normal space. Gaussian random fields are defined with zero mean and 0.5 variance. Final property fields are recentered and converted back to physical units using their respective transformations.

S-STBM requires an objective function that quantifies the misfit between simulated and observed system responses. Here, we adopt a Bayesian framework to define the OF, explicitly accounting for uncertainty in field observations. In Bayesian terms, the inverse problem consists of obtaining samples from the posterior distribution of models $f(m|d)$ conditioned on a set of observed state data d:

$$f(m|d) \propto f(d|m)f(m) \tag{1}$$

In this formulation, the prior distribution $f(m)$ represents the *a priori* distribution of the hydraulic conductivity and drawdown profiles, while the likelihood function $f(d|m)$ defines the probability of observing the measured state variables d given a specific model m. The likelihood thus quantifies the discrepancy between simulated and observed flow rates, whereas the prior distribution accounts for deviations between the simulated and *a priori* fracture hydraulic conductivities ($f(m_f)$) and between the simulated and *a priori* drawdowns ($f(m_h)$). In our implementation, m_f and m_h are assumed to be independent.

Multivariate normal probability density functions are used as priors for m_f, while a uniform distribution is applied for m_h. The log-hydraulic conductivity profiles are modeled using multivariate normal probability density functions, and the residuals between simulated and observed flow rates are assumed to follow a multivariate normal distribution with zero mean and a diagonal variance–covariance matrix. This formulation explicitly incorporates the uncertainties in field observations into the OF. In this study, the diagonal variance–covariance matrix was constructed so that each diagonal element represents a variance equal to the square of 10 % of the corresponding measured flow rate. This formulation implies that the uncertainty associated with each observation is proportional to its magnitude, and that the algorithm considers simulated flow rates acceptable when they fall within ±10 % of the observed values.

During calibration, it was observed that the hydraulic conductivity of the first fracture exerted a disproportionately large influence on the optimization process. Because this fracture affects all simulated flow rates, the algorithm tended to focus on fitting its hydraulic conductivity while neglecting the fractures located lower down in the borehole. To address this issue, a weighting vector (w) was introduced into the hydraulic conductivity term of the OF. This weighting ensures that fractures with greater influence on the total flow remain closer to their *a priori* values, while fractures located deeper in the borehole, whose influence is smaller, are allowed greater variability. This adjustment improves the overall balance of the inversion and prevents early fractures from dominating the calibration process. The final OF is formulated in log-space for mathematical simplicity:

$$OF = -log\left[\sum_i f\left(m_{f,i}\right) \cdot w + \sum_i f\left(m_{h,i}\right) + f(d|m)\right] \tag{2}$$

3. Results and discussion

The motivation for applying a geostatistical inversion in this study arises from the intrinsic coupling between hydraulic and thermal processes in fractured aquifers. Because the thermal response of a SCW is highly sensitive to subsurface flow conditions, reliably predicting geothermal performance requires hydraulic conductivity profiles that realistically capture the spatial variability of fracture properties. To improve this understanding, we develop a framework to quantify the information content of data routinely collected during exploratory drilling. This framework assimilates flow rate measurements acquired during drilling to reconstruct fractured hydraulic conductivity profiles and to evaluate how these profiles influence the system's thermal response. A stochastic approach is particularly valuable here, as it provides quantitative measures of uncertainty and allows assessing the robustness of the inferred properties.

To demonstrate the capabilities of the proposed framework, the section is divided into two parts. The first examines a synthetic scenario designed to evaluate the accuracy of the inversion in recovering known hydraulic conductivity profiles and its impact on simulated transfer functions. The second applies the methodology to a real case, allowing us to assess its performance under field conditions and to explore the geothermal implications of the inferred hydraulic conductivity profile.

3.1. Synthetic case

Figure 3 presents the results of 100 independent geostatistical realizations for the synthetic case. Overall, the mean simulated flow rates reproduce the reference profile with very good accuracy. Although a few realizations fall outside the ±10 % error margin, the majority remain within this range. The sharp change in flow rate observed after 57.15 m highlights how different realizations optimized the flow response at slightly varying depths. Some realizations reproduced this increase near 64.77 m, while others delayed it until 72.39 m. This variability suggests that an increase in fracture hydraulic conductivity occurs near 60 m depth.

This interpretation is supported by the top-right panel, where the fracture at 64.77 m shows a marked deviation from the *a priori* value. It is also the depth interval displaying the greatest scatter among realizations, indicating that while most simulations captured the flow rate transition between 57.15 m and 64.77 m, others underestimated the fracture conductivity at that level and compensated by assigning higher values in subsequent intervals. These observations underline the importance of performing multiple realizations of the same numerical model to minimize the influence of outliers on the mean result. Nevertheless, the S-STBM algorithm successfully identified this fracture as one of the most poorly represented by the *a priori* model.

The mean estimated fracture hydraulic conductivities diverge from the *a priori* values over the upper 80 m of the borehole, then progressively converge toward them at greater depths. This pattern arises because, as discussed previously, the shallow fractures exert a disproportionately large influence on the simulated flow rate due to their hydraulic position within the model domain. Despite the application of a weighting vector, these upper fractures remain preferentially optimized. Beyond approximately 80 m depth, the close agreement between the mean realizations and the *a priori* values indicates that the S-STBM algorithm converges toward a near-zero mean in the assumed normal distribution, signifying limited potential to further improve the fit between simulated and reference flow rates at these depths.

The reference fracture hydraulic conductivity profile remains within the range of the ensemble of realizations, despite diverging from the *a priori* values, and the mean estimated profile successfully captures its primary trends, as reflected by a correlation factor of 0.82. Over the upper 80 m, the mean of the realizations accurately identifies intervals where the *a priori* values are over- or underestimated, providing insight into the relative distribution of lower- and higher-permeability zones.

Because drawdown was constrained only by imposed bounds rather than by a fixed reference profile, some discrepancies between the mean simulated drawdown and the reference distribution are expected. Nevertheless, it is desirable that the reference data lie within the 90 % confidence interval to minimize the influence of outlier values. A clear relationship emerges between drawdown and flow rate: realizations exhibiting lower drawdown consistently correspond to lower flow rates, and vice versa. These observations are illustrated by the color grading in the two left panels of Figure 3, where the blue–yellow gradient highlights this trend. This observation underscores the importance of accurately representing drawdown evolution, as it strongly influences the simulated flow response. In contrast, no systematic relationship is observed for the OF, by mathematical relation, nor for fracture hydraulic conductivities.

As for the OF, its mean decreases rapidly during the initial iterations, with improvements becoming progressively smaller after approximately five iterations. For this study, 30 iterations were retained to ensure convergence, although the algorithm generally began to optimize noise around the 20th iteration.

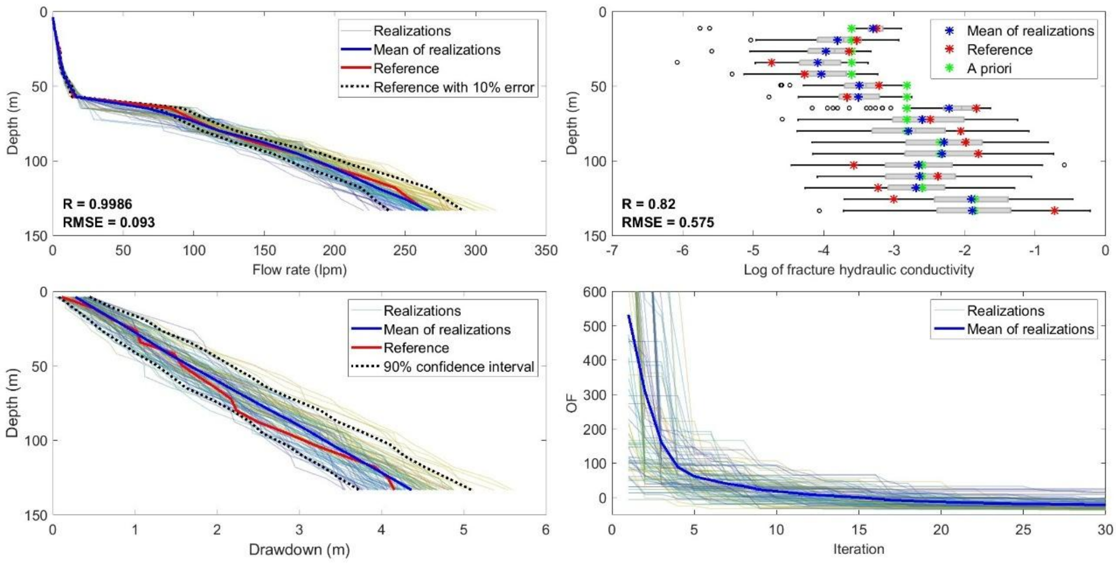

Figure 3. Simulation results from 100 realizations of the synthetic case. Top left: Flow rates. Top right: Fracture hydraulic conductivities. Bottom left: Drawdown. Bottom right: Objective function. Each realization is consistently color-coded across all panels to facilitate comparison.

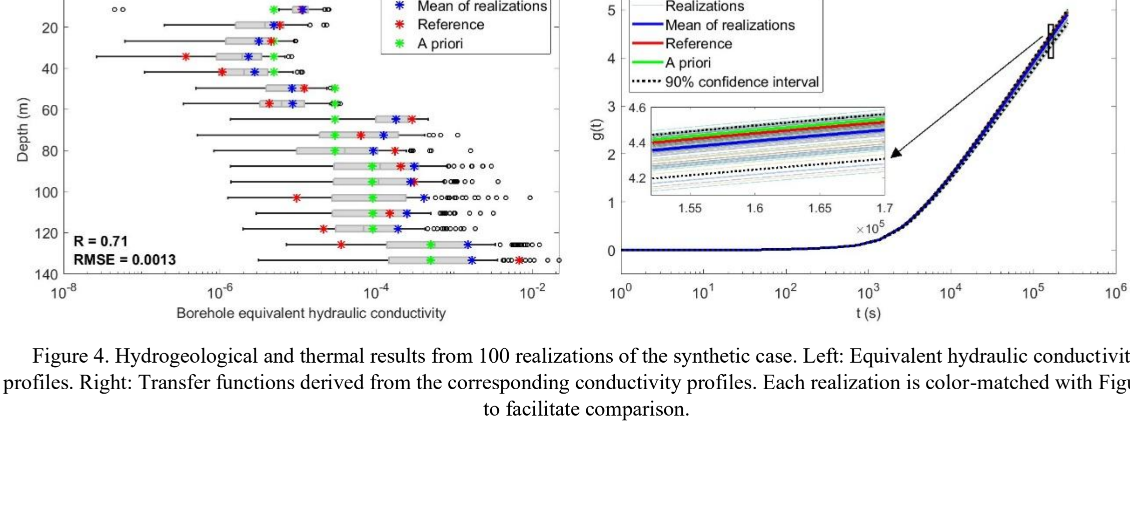

Figure 4. Hydrogeological and thermal results from 100 realizations of the synthetic case. Left: Equivalent hydraulic conductivity profiles. Right: Transfer functions derived from the corresponding conductivity profiles. Each realization is color-matched with Figure 3 to facilitate comparison.

Figure 4 presents the evolution of the borehole equivalent hydraulic conductivity, accounting for both fracture apertures and rock matrix hydraulic conductivity. The mean of realizations tracks the reference profile more closely than the *a priori* distribution for the first 100 m, demonstrating that the S-STBM algorithm can adjust the initial parameterization to better reproduce the hydraulic structure of the reference data. Unlike the fracture hydraulic conductivities shown in Figure 3, the equivalent hydraulic conductivity exhibits a clear distinction between the *a priori* values and the mean of realizations along the entire borehole. This indicates that even when the mean fracture hydraulic conductivities do not significantly deviate from the *a priori*, the inclusion of additional hydrogeological parameters allows the mean of realizations to deviate from the *a priori* at greater depths. Notably, numerous outliers are observed over the same depth interval, reflecting realizations that substantially overestimate the equivalent hydraulic conductivity relative to the *a priori*. These extreme values help bring the mean closer to the reference, particularly for the deepest fracture, where the reference itself falls within the outlier range.

Fracture hydraulic conductivities have a noticeable impact on the evolution of the transfer functions. Within a given numerical model, variations in these conductivities result in a range of possible transfer function values, g(t). After simulating g(t) for a three-day period, the difference between the minimum and maximum g(t) reaches 8.3 %. Despite this variability, the right panel of Figure 4 shows that the reference data, the mean of realizations, and the *a priori* values are all very similar. The maximum relative error between the mean of realizations and the reference is only 1.19 %. This close agreement indicates that, even before inversion, a well-informed *a priori* characterization of hydrogeological parameters can provide an accurate estimate of the transfer function.

A limitation of these results is that the reference data are derived from the same *a priori* parameters used in the simulations. Consequently, the realizations were inherently constrained to lie within a similar range as the reference. In practical cases where the reference is unknown for fracture hydraulic conductivities and drawdown, the influence of the *a priori* becomes more critical and should be carefully assessed.

3.2. Real scenario

For this series of simulations, in which only the reference flow rate data were available, the results illustrate how the methodology developed in this study could be applied to real data. Figure 5 presents the outcomes of 100 realizations for the real scenario. The reference flow rate profile exhibits a more complex evolution than in the synthetic case, yet the S-STBM algorithm successfully reproduces its general trend, with the mean of realizations remaining close to the observed data despite inherent uncertainties.

The pronounced decrease in flow rate observed between 87.63 m and 102.87 m is most likely the result of simplifications made during data acquisition rather than a genuine geological feature, as a 15 m interval devoid of conductive fractures would be improbable in this context. Consequently, a larger number of realizations fall outside the ±10 % error margin within this depth range. This discrepancy may also be attributed to the limited information available on drawdown, whose evolution was assumed to follow that of the flow rate. Compared with the synthetic scenario, the correlation between drawdown increases and flow rate response appears less distinct in the real case, reflecting the higher complexity and uncertainty associated with drawdown behavior under real drilling conditions.

As for the fracture hydraulic conductivity, some observations are consistent with those made for the synthetic case. The shallow fractures are again preferentially optimized, while at greater depths (> 70 m), the S-STBM algorithm tends to converge toward a near-zero mean in the assumed normal distribution. In the synthetic scenario, the weighting vector limited the range of possible values for the upper fractures, allowing this range to increase progressively with depth. In contrast, in the real case, even with the weighting vector applied, all fractures appear to share a similar range of possible values, with the shallowest ones exhibiting the largest variability.

Furthermore, none of the means of realizations are significantly lower than their associated *a priori*, suggesting that the *a priori* fracture conductivities may have been generally underestimated. This may also indicate that the weighting vector was insufficiently strong to constrain the optimization of the upper fractures in a context where the flow rate evolution is both more complex and of greater magnitude.

The behavior of the simulated drawdowns may further explain why the inferred fracture hydraulic conductivities show less distinct patterns than in the synthetic case. In the synthetic scenario, the drawdown evolution was predefined and well understood, whereas in the real case, no reference data were available to assess whether the simulated drawdowns were realistically characterized. Since the shape of the flow rate curve is strongly influenced by drawdown variations, an incomplete understanding of this relationship may have led the algorithm to compensate by adjusting the fracture hydraulic conductivities based on an inaccurate assumption.

Regarding the OF, its evolution follows a trend similar to that observed in the synthetic scenario. Although the real case exhibits less variability in the initial iterations, it does not achieve the same minimum OF values after 30 iterations. This difference can be partly attributed to the distinct CDF used in the real case, which introduces a constant term in the OF formulation ($f(m_h)$) larger than that of the synthetic scenario. Moreover, this behavior reflects a context where less information is available and where the *a priori* parameters may not accurately represent the reference conditions, thereby limiting the algorithm's ability to minimize the OF further.

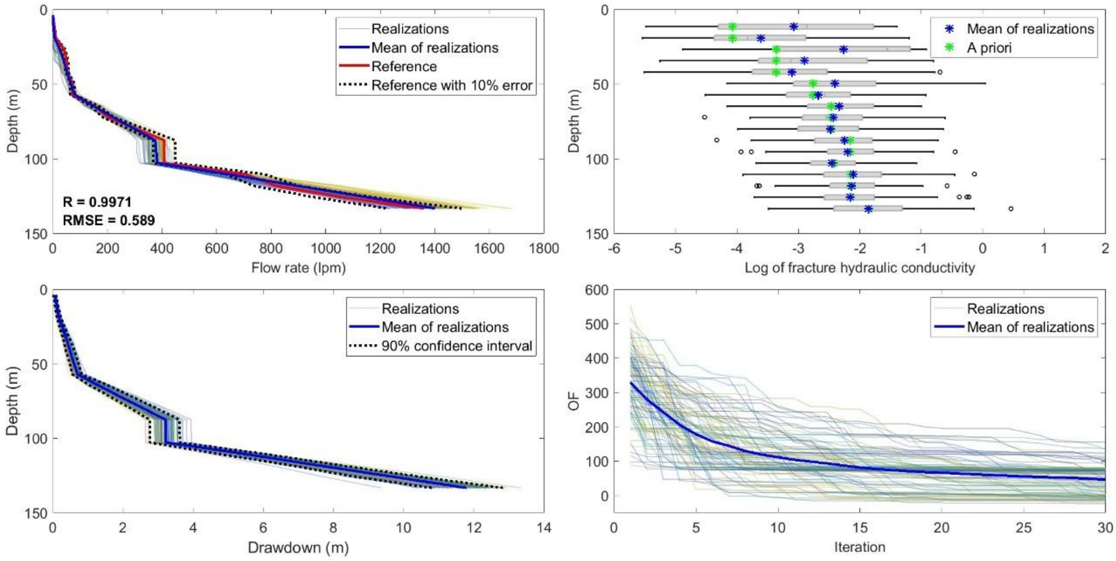

Figure 5. Simulation results from 100 realizations of the real case. Top left: Flow rates. Top right: Fracture hydraulic conductivities. Bottom left: Drawdown. Bottom right: Objective function. Each realization is consistently color-coded across all panels to facilitate comparison.

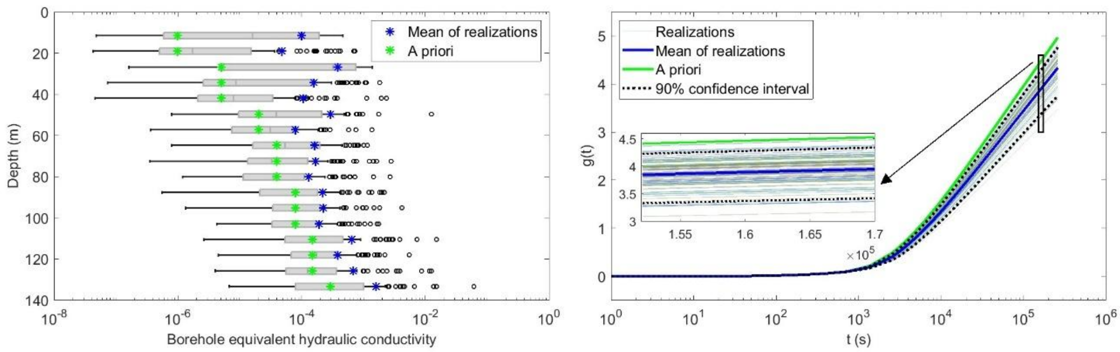

Figure 6. Hydrogeological and thermal results from 100 realizations of the synthetic case. Left: Equivalent hydraulic conductivity profiles. Right: Transfer functions derived from the corresponding conductivity profiles. Each realization is color-matched with Figure 3 to facilitate comparison.

Figure 6 presents the equivalent hydraulic conductivity profiles and the corresponding thermal transfer functions for the real scenario. The left panel shows that the *a priori* values are systematically lower than the mean of realizations, suggesting that the fractured rock mass may be more permeable than initially expected. A substantial number of outliers appear across nearly all depths, indicating that, in the real scenario, the realizations more readily adopted extreme conductivity values that deviated noticeably from the *a priori*, particularly toward higher values, compared to the synthetic case. This behavior may result from the variance selected for the S-STBM algorithm, which could have allowed unrealistically large fluctuations in fracture hydraulic conductivities. Alternatively, it may indicate that the *a priori* values were themselves underestimated and that several realizations successfully departed from these initial assumptions to obtain hydraulic conductivity distributions that better reproduced the observed flow behavior.

As shown in the right panel of Figure 6, the distinction between the *a priori* and the inferred equivalent hydraulic conductivity profiles translates directly into the thermal response: the a priori transfer function lies entirely outside the range of g(t) values obtained for the real scenario. This demonstrates that the S-STBM algorithm identified a set of fracture hydraulic conductivities significantly higher than those assumed initially, leading to a considerably different thermal behavior of the borehole. While the influence of the assumed drawdown must be acknowledged, these results collectively suggest that the lithologies intersected by the borehole are more permeable than typical values reported for these rock types.

Both scenarios were assigned similar *a priori* fracture hydraulic conductivities, with the synthetic case representing a more fractured aquifer. The substantially higher flow rates measured in the real scenario compared with the synthetic one already pointed toward a more conductive system, an inference that is consistent with, and further reinforced by, the S-STBM results.

Conclusion

This study investigated the use of flow rate data acquired during drilling to infer the vertical distribution of hydraulic conductivity in fractured rock using a geostatistical inversion framework. By applying the S-STBM algorithm to both synthetic and real datasets, the methodology demonstrated its ability to recover representative patterns of hydraulic conductivity and flow evolution, even when limited information is available. The synthetic case validated the approach by showing a strong correspondence between the reconstructed and reference profiles, while the real case highlighted the practical challenges associated with measurement uncertainties and the absence of direct drawdown data. Despite these limitations, the results confirm that flow rate measurements collected during drilling contain valuable hydrogeological information that can be extracted through probabilistic inversion techniques.

This work contributes to the ongoing effort to reduce uncertainty in geothermal system design by introducing a non-intrusive, cost-effective addition to conventional testing that enhances the resolution of subsurface property distributions. The overall objective is to improve the prediction of heat transfer processes in fractured rock aquifers, thereby enhancing the design reliability of SCWs and other open-loop systems and ultimately reducing the financial and logistical constraints associated with detailed field campaigns.

Future research should focus on improving the characterization of drawdown behavior during drilling, as this parameter was shown to strongly influence the inversion results. Future work should also focus on improving the representation of drawdown dynamics during drilling, particularly by simulating multiphase flow conditions to account for the combined effects of air and water injection in air-drilled boreholes. Incorporating these processes would provide a more realistic assessment of pressure and flow rate evolution, thereby refining the estimation of fracture hydraulic properties and improving the robustness of the inversion methodology. Ultimately, the methodology developed here provides a foundation for more accurate and economically viable geothermal resource assessments in fractured rock environments.

Acknowledgements

This research was made possible by a Canada Graduate Scholarships-Master's (CGS M) from the Natural Sciences and Engineering Research Council of Canada (NSERC) of O. Brisebois and a NSERC grant (ALLRP 544477-19).

References

[1] Scheidt C, Li L, Caers J. *Quantifying Uncertainty in Subsurface Systems*. Hoboken, USA: John Wilry & Sons, Inc.; 2018.
[2] Li ZW, Feng XT, Zhang YJ, Xu TF. Effect of hydrological spatial variability on the heat production performance of a naturally fractured geothermal reservoir. *Environmental Earth Sciences*. 2018;**77**(496).
[3] Butler Jr J, Xiaoyong Z. Hydraulic tests in highly permeable aquifers. *Water Resources Research*. 2004;**401**(12).
[4] Illman WA. Hydraulic Tomography Offers Improved Imaging of Heterogeneity in Fractured Rocks. *Groundwater*. 2013;**52**(5):659–84.
[5] Maliva RG. *Hydraulic Conductivity Estimation and Upscaling*. Champ, Switzerland: Springer; 2016.

[6] Tsang CF, Neretnieks I. Flow channeling in heterogeneous fractured rocks. *Reviews of Geophysics*. 1998;**36**(2):275–98.
[7] Neuman SP. Trends, prospects and challenges in quantifying flow and transport through fractured rocks. *Hydrogeology Journal*. 2005;**13**:124–47.
[8] Williams JH, Johnson CD. Acoustic and optical borehole-wall imaging for fractured-rock aquifer studies. *Journal of Applied Geophysics*. 2004;**55**(1-2):151-9.
[9] Legchenko A, Baltassat JM, Beauce A, Bernard J. Nuclear magnetic resonance as a geophysical tool for hydrogeologists. *Journal of Applied Geophysics*. 2002;**50**(1–2):21–46.
[10] Perdomo S, Ainchil JE, Kruse E. Hydraulic parameters estimation from well logging resistivity and geoelectrical measurements. *Journal of Applied Geophysics*. 2014;**105:**50–8.
[11] Seto K, Hollenshead JT, Watson AT, Chang CTP, Slattery JC. Determination of Permeability Distributions Using NMR Velocity Imaging. *Transport in Porous Media*. 2001;**42:**351–87.
[12] Manivannan S, Bérest P, Jacques A, Brouard B, Jaffrezic V, De Greef V.,2019.
"Permeability Logging through Constant Pressure Injection Test: In-Situ Methodology and Laboratory Tests," SPE Annual Technical Conference and Exhibition. Calgary, Canada, paper # SPE-196116-MS.
[13] Pasquier P, Nguyen A, Eppner F, Marcotte D, Neaudron P. Standing column wells. In: Rees SJ, editor. *Advances in Ground-Source Heat Pump Systems*. Woodhead Publishing; 2016. p. 269–94.
[14] Spitler JD, Rees SJ, Deng Z, Chiasson A, Orio CD, Johnson C. R&D studies applied to standing column well design. *ASHRAE research project*. 2002;1–123.
[15] Nguyen A, Pasquier P, Marcotte D. Influence of groundwater flow in fractured aquifers on standing column wells performance. *Geothermics*. 2015;**58**:39–48.
[16] Marcotte D, Pasquier P. Fast fluid and ground temperature computation for geothermal ground-loop heat exchanger systems. *Geothermics*. 2008;**37**(6):651–5.
[17] Rose C, Pasquier P, Nguyen A, Labib R. Efficient construction of short-term transfer functions for closed-loop boreholes in stratified aquifers under groundwater flow using neural networks and wavelet decomposition. *Science and Technology for the Built Environment*. 2025;**42**:1–17.
[18] Nguyen A, Jacques L, Pasquier P. An easy-to-use analytical model for standing column wells operating with bleed. *Applied Thermal Engineering*. 2025;**258**(A).
[19] Beaudry G, Pasquier P, Marcotte D. The impact of rock fracturing and pump intake location on the thermal recovery of a standing column well: model development, experimental validation, and numerical analysis. *Science and Technology for the Built Environment*. 2019;**25**(8):1052–68.
[20] Robert S, Pasquier P, Nguyen A. Impact of layered heterogeneity on thermal response test interpretation performed on a standing column well operated without bleed. *Geothermics*. 2022;**101**.
[21] Lauzon D, Marcotte D. Calibration of random fields by a sequential spectral turning bands method. *Computers & Geosciences*. 2020;**135**.
[22] Globensky Y. *Géologie des Basses-Terres du Saint-Laurent, Report MM, 02-85*. Québec: Ministry of Energy and Resources, General Direction for Geologic and Mineral Exploration; 2016.
[23] COMSOL AB. COMSOL Multiphysics v. 6.0. Stockholm, Sweden; 2021.
[24] Thiem G. *Hydrologische methoden*. Leipzig, Germany: J. M. Gebhardt; 1906. 56 p.
[25] Nasr M. *Évaluation des propriétés thermiques de la plateforme du Saint-Laurent: mesures au laboratoire et approche diagraphique* (Master's thesis). Québec, Canada: Université du Québec, Institut national de la recherche scientifique; 2016.
[26] Emery X, Arroyo D, Porcu E. An improved spectral turning-bands algorithm for simulating stationary vector Gaussian random fields. *Stochastic Environmental Research and Risk Assessment*. 2015;**30**:1863–73.
[27] Nastev M, Savard MM, Lapcevic P, Lefebvre R, Martel R. Hydraulic properties and scale effects investigation in regional rock aquifers, south-western Quebec, Canada. *Hydrogeology Journal*. 2004;**12**:257–69.
[28] Tran Ngoc TD, Konstantinovskaya E, Lefebvre R, Malo M. *Caractérisation hydrogéologique et pétrophysique des aquifères salins profonds de la région de Bécancour pour leur potentiel de séquestration géologique du CO2, Rapport INRSCO2-2011-V2.10*. Québec: INRS - Centre Eau Terre Environnement; 2011.
[29] Lauzon D. A U-Net architecture as a surrogate model combined with a geostatistical spectral algorithm for transient groundwater flow inverse problems. *Advances in Water Resources*. 2024;**189**.